Full Text View

Volume 32, Issue 6 (June 2002)

Journal of Physical Oceanography
Article: pp. 1824–1837 | Abstract | PDF (4.14M)

Interannual Variability in the Eastern Subtropical North Pacific Ocean

Alan P. Leonardi

Earth System Science Interdisciplinary Center, University of Maryland, College Park, Maryland

Steven L. Morey and James J. O'Brien

Center for Ocean–Atmospheric Prediction Studies, The Florida State University, Tallahassee, Florida

(Manuscript received November 13, 2000, in final form November 2, 2001)

DOI: 10.1175/1520-0485(2002)032<1824:IVITES>2.0.CO;2

ABSTRACT

Interannual variability in the eastern subtropical North Pacific Ocean is investigated using the Naval Research Laboratory Layered Ocean Model (NLOM). Emphasis is placed on examining the nature of westward propagating Rossby waves and their interaction with the overlying atmosphere.

Singular value decomposition (SVD), complex empirical orthogonal function (CEOF), and multichannel singular spectrum (M-SSA) analyses are used to isolate the standing and propagating response due to modeled Rossby waves and observed wind stress curl (WSC) anomalies as well as their dominant frequencies of oscillation, respectively. In addition to a large-scale interdecadal fluctuation, two distinct forms of Rossby waves are found to exist, one wind forced and the other freely propagating.

SVD and CEOF analyses of NLOM upper layer thickness anomalies suggest a leading order source of variability stemming from a large-scale interdecadal fluctuation. M-SSA analysis also depicts this low frequency mode, but to a lesser extent and at higher order. The modeled temporal coverage limits the extent to which this feature can be studied further.

Of primary interest in the eastern subtropical North Pacific Ocean are large-scale interannual wind-forced Rossby wave variations. Independent M-SSA analysis of modeled ULT and observed WSC anomalies suggests a low frequency (~ 51 month period) atmospherically forced ocean response in which westward atmospheric propagation leads forced oceanic

Rossby wave propagation by roughly 3 months. In addition to this low frequency forced oceanic wave response with a phase speed of $c_r \sim 12$ cm s^{-1}, a distinct freely propagating biennial oceanic Rossby wave is also found to exist, with a phase speed of $c_r \sim 8$ cm s^{-1}, emanating from El Niño–Southern Oscillation related coastally trapped Kelvin waves.

1. Introduction

Since Stommel (1957), and later White and McCreary (1974), investigated the response of the interior ocean to changes in the overlying atmosphere, numerous investigators have examined Pacific Ocean thermocline variability on time scales of seasons to decades (Meyers 1975; White 1977, 1978; Meyers 1979; Kang and Magaard 1980; Magaard 1983; White et al. 1985; Kessler 1990; Qiu et al. 1997; White and Cayan 2000, and references therein). An integral component of these studies focused on observing and explaining large-scale westward propagating Rossby waves and their interaction with the overlying atmosphere. This research addresses wind forced Rossby waves as they pertain to the midlatitude Eastern North Pacific.

The foundations of the above studies are rooted in theory (Stommel 1957; White and McCreary 1974). Meyers (1975) provided the first clear observational evidence for Pacific ocean–atmosphere interaction by relating annual thermocline fluctuations to the annual cycle in wind stress curl (WSC) near the Pacific North Equatorial Current. Using an augmented dataset that included both mechanical bathythermographs and expendable bathythermographs (MBTs and XBTs), White (1977) extended the f-plane dynamics of Meyers (1975) arguing the thermocline variability to be strongly influenced by β-plane dynamics. In this work, White (1977) first suggests a westward propagating long wave, composed of a local forced response and a freely propagating response, with a phase speed twice that of nondispersive Rossby waves ($C = 2C_R$).

White (1977), however, did not include either an alongshore wind or equatorially forced, coastally propagating Kelvin waves. These limitations can be avoided by moving to a point west of the eastern boundary layer and using observed thermocline variations as the boundary condition for the model. Using this technique, Meyers (1979) successfully separated Ekman pumping variability observed along 12°N from the combined Ekman pumping/Rossby wave mode seen along 6°N, suggesting larger than expected Rossby wave phase speeds might be better understood if interaction between the annual waves and mean shear flow is allowed.

Following these initial investigations, further observational studies revealed a strong annual Rossby wave dominance in the North Pacific between 30° and 40°N while variations encompassing the entire spectrum are seen between 5° and 30°N with strong peaks in the interannual band (with 4 and 6.7 yr periods: Kang and Magaard 1980; Magaard 1983; Kessler 1990). Using a quasigeostrophic (QG) model of thermocline variations dependent upon Ekman pumping and Rossby wave radiation, Kessler (1990) notes the largest interannual WSC forcing exists in midbasin (between 15° and 30°N, 175° and 110°W) with little annual variation over the same region. The simple QG model performs well along 5°N (in agreement with Meyers 1979) and between 14° and 18°N for annual variations and poleward of 15°N for interannual variations, but with mixed interannual results equatorward of 15°N.

During the time Kessler (1990) was analyzing BT data, Chelton and Schlax (1996) produced a set of altimetrically derived global observations of oceanic Rossby waves highlighting the systematic differences between observed and predicted Rossby wave phase speeds, and spawning a wide array of studies aimed at its understanding. Among these were observational and theoretical works attributing the enhanced propagation speeds to interactions between the waves and the background mean flow (Killworth et al. 1997; Dewar 1998), to eddy dissipation (Qiu et al. 1997), and to ocean–atmosphere interactions (e.g., Miller et al. 1997; White et al. 1998; White 2000). For each independent process, the Rossby wave phase speed modifications are of the right size and orientation to account for the observed discrepancies.

Recent evidence also implies large-scale atmosphere–ocean coupling exists on biennial to interdecadal timescales (Miller et al. 1997; White et al. 1998; Tourre et al. 1999; White and Cayan 2000; White 2000). Miller et al. (1997) suggests interior ocean interannual variability is dominated by large-scale wind stress curl anomalies associated with atmospheric Pacific North American pattern fluctuations, while White et al. (1998) and White (2000) reveal large-scale coherent propagating patterns in both atmospheric (WSC, meridional wind stress) and oceanic (sea level height, sea surface temperature) fields in both the Tropics and extratropics. The observational and theoretical evidence suggests a plausible link between the atmosphere and ocean on interannual timescales.

Motivated by the above works, this work is aimed at examining the interaction between the WSC and westward, freely propagating Rossby waves in the eastern subtropical North Pacific Ocean. Like many previous authors, the understanding relies upon low frequency (QG) dynamics, but which, to the best of the authors knowledge, is addressed for the first time

using a high-resolution, nonlinear numerical ocean model with realistic forcing. Unlike purely observational studies, a numerical model can be used to isolate the dynamical mechanisms involved in the variability, while alleviating the limitations of QG dynamics and observations alone (see above; Kessler 1990).

It will be shown in these model results that although coastally generated westward freely propagating Rossby waves exist in the latitude band 18°–24°N, interannual variability is mainly due to large-scale wind stress curl fluctuations that force oceanic Rossby waves with propagation speeds roughly twice that of linear theory. While the possibility of a longer interdecadal mode of variability is noted, the model runs lack sufficient length to examine them in detail. Their validation and physical implications are left to a future study. Section 2 presents the numerical ocean model used in this work with a brief discussion of the model wind forcing as well as comparison with observations. Theory for and existence of the subtropical eastern North Pacific variability is presented in section 3 with a discussion and synthesis of the results presented in section 4.

2. Numerical model and observational data

a. Eddy-resolving general circulation model

The primitive equation layered ocean model utilized in this study, the Naval Research Laboratory Layered Ocean Model (NLOM), is a descendent of the model by Hurlburt and Thompson (1980) with enhanced processing and capability (Wallcraft 1991). The vertically integrated equations used in the current version of the NLOM n-layer, finite depth, hydrodynamic model are

$$\begin{aligned}
&\frac{\partial \mathbf{V}_k}{\partial t} + (\boldsymbol{\nabla}\cdot\mathbf{V}_k + \mathbf{V}_k\cdot\boldsymbol{\nabla})\mathbf{v}_k + \mathbf{k}\times f\mathbf{V}_k \\
&\quad = -h_k\sum_{l=1}^{n} G_{kl}\boldsymbol{\nabla}(h_l - H_l) + \frac{(\boldsymbol{\tau}_{k-1} - \boldsymbol{\tau}_k)}{\rho_0} \\
&\qquad + \max(0, -\omega_{k-1})\mathbf{v}_{k-1} \\
&\qquad - [\max(0, \omega_{k-1}) + \max(0, -\omega_k)]\mathbf{v}_k \\
&\qquad + \max(0, \omega_k)\mathbf{v}_{k+1} + \max(0, -C_M\omega_{k-1})(\mathbf{v}_{k-1} - \mathbf{v}_k) \\
&\qquad + \max(0, C_M\omega_k)(\mathbf{v}_{k+1} - \mathbf{v}_k) + A_H\nabla^2\mathbf{V}_k \\
&\frac{\partial h_k}{\partial t} + \boldsymbol{\nabla}\cdot\mathbf{V}_k = \omega_k - \omega_{k-1}, \qquad (1)
\end{aligned}$$

where, $k = 1, \cdots, n$ when referring to layers, and $k = 0, \cdots, n$ when referring to interfaces between layers with $k = 0$ at the surface. For a full description of the model and notation used above, see Metzger and Hurlburt (1996) and Shriver and Hurlburt (1997).

The model has no-slip and kinematic boundary conditions and is solved on a C grid (Mesinger and Arakawa 1976) using a semi-implicit scheme for finite depth simulations, and an explicit scheme for reduced gravity experiments. The model includes a free surface and the barotropic mode. A more detailed description of the model is given by Wallcraft (1991) and Shriver and Hurlburt (1997).

Although thermodynamic versions of the model exist, only results from a single hydrodynamic, six-layer, finite depth simulation are presented here. The only forcing used in this experiment is the applied wind stress, a hybrid composed of Hellerman and Rosenstein (1983, hereafter HR) monthly climatology and the European Centre for Medium-Range Weather Forecasts (ECMWF 1995) 1000-mb 12-hourly winds. The data are constructed by replacing the ECMWF climatological mean for 1981–1996 with that of the HR dataset, effectively producing a wind stress with both realistic variability and climatology. The ECMWF/HR pseudostress data is multiplied by a constant drag coefficient, $C_D = 1.5 \times 10^{-3}$, and the air density at sea level, $\rho_a = 1.2$ kg m^{-3}, to obtain the wind stress. When processed in this manner, the ECMWF and HR wind stresses have nearly identical mean and standard deviations over the model domain and provide the most realistic model

results over the domain, eastern subtropical Pacific, and the equatorial Pacific collectively (for details, see Hurlburt et al. 1996; Hundermark et al. 1999; Hackert et al. 2001; Zamudio et al. 2001).

A realistic coastline and bottom topography are included by utilizing a modified version of the 1/12° ETOP05 (NOAA 1986) bottom topography with extensive corrections to the geometry of the Hawaiian Islands and several semienclosed seas in the Western Pacific Ocean. The ETOP05 data are interpolated to the model grid and twice smoothed using a nine-point smoother. The smoothing is designed to reduce energy generation at smaller scales.

The 200-m isobath (near the shelf break) represents the minimum depth in the model and is used as the model boundary. The only exceptions to this are regions where shallower depths are needed to connect semienclosed seas to the Pacific Ocean (e.g., the Tsugaru, Tsushima, and Soya Straits connecting the Sea of Japan to the Pacific Ocean).

The maximum depth of the model is 6500 m and seamounts and other rough bottom topography are confined to the lowest layer. As a result, numerical difficulties arising when moving interfaces and sloping topography intersect are removed (Hurlburt and Thompson 1980). The two primary reasons for including topographic features are to force the lowest layer (abyssal) flow to follow the f/h contours and to regulate baroclinic instability. The confinement of topography to the lowest layer has negligible impact on these. Additionally, flow through straits and over shallow sills is constrained to small values below the sill depth.

The model domain is the Pacific Ocean from 20°S to 62°N and ~109°E to ~77°W with a horizontal resolution of 1/16° × 45/512° (latitude × longitude). Since the model boundaries at 20°S and Indonesia are treated as closed, there is no Indonesian throughflow and no contribution from the global thermohaline circulation. Finally, in an effort to reduce the overall size of the dataset, the NLOM data is subsampled, and if not residing on an integer line of longitude or latitude linearly interpolated, to form a 1° × 1° grid that retains the spatial scales of interest.

The model outputs data every 3.05 days. However, since the timescales of interest here are interannual, monthly means are created and examined from January 1981 through December 1996. The basic large-scale model phenomenology is the same as that of Jacobs et al. (1994), Metzger and Hurlburt (1996), Hurlburt et al. (1996), Mitchell et al. (1996), Murray et al. (2001), and Leonardi et al. (2001, manuscript submitted to *J. Geophys. Res.*). Therefore, a detailed description of the basin-scale flow is not provided here. Instead, a simple empirical orthogonal function (EOF) analysis is performed revealing strong agreement between both annual (Fig. 1) and interannual (not shown) cycles of monthly NLOM modeled and TOPEX/Poseidon (T/P; Subrahmanyam 1998; Zamudio et al. 2001) observed sea surface height (SSH) measurements. For a more detailed description of the large-scale flow and comparison with observations, the reader is encouraged to consult the references noted above.

3. Results

A simple analytical model is employed to examine the interannual variability in the eastern North Pacific subtropical gyre. Although Kessler (1990) (and Meyers 1975; White 1977, 1978; Meyers 1979; beforehand) used a simple quasi-geostrophic model to examine thermocline fluctuations, the isopycnal nature of the model used here allows similar analysis of the modeled upper-layer thickness (White 1978; Meyers 1979; Qiu et al. 1997). Applying a few simple assumptions to the generalized Navier–Stokes equations reduces the horizontal equations of motion to

$$-fv = -g'\frac{\partial h}{\partial x} + \frac{\tau_w^x}{\rho H} \qquad fu = -g'\frac{\partial h}{\partial y} + \frac{\tau_w^y}{\rho H} \qquad (2)$$

and the continuity equation to

$$\frac{\partial h}{\partial t} + H\left(\frac{\partial u}{\partial x} + \frac{\partial v}{\partial y}\right) = 0, \qquad (3)$$

where all variables are standard oceanic variables representing the zonal and meridional currents (u and v, respectively) and wind stress (τ^x_w and τ^y_w), coriolis parameter (f), time varying and resting upper layer thickness (h and H), density (ρ), and reduced gravity ($g' = g\Delta\rho/\rho$).

The above equations can be further reduced by cross differentiation and elimination of the divergence term via the continuity equation. The result,

$$\frac{\partial t}{f^2}\frac{\partial x}{\rho f'} \qquad (4)$$

is the low frequency long-wave equation representing changes in the upper-layer thickness (or analogously, the thermocline depth) brought about by Rossby wave propagation and Ekman pumping. Here, $\beta = \partial f/\partial y$.

It is important to note that the above equations require negligible local accelerations (the common low-frequency limit, long-wave approximation: see Gill 1982). Under this assumption, solutions to Eq. (4) are latitudinally dependent with each latitude independent of the others and long planetary waves nondispersive with westward phase speeds dependent on the layer thickness, $c = (g'H)^{1/2}$.

Although Eq. (4) is a simple relationship for (externally) forced time-dependent β-plane dynamics, the analytical model limitations (Kessler 1990) have negligible impact on the overall nature of the solution. Additionally, while vertical and horizontal shear effects can produce modified Rossby wave phase speeds (Killworth et al. 1997; Dewar 1998), both have minimal effect over the subtropics. Since the focus here is primarily on the effects of large-scale subtropical WSC, the simple equation presented above is a valuable tool for determining the interannual response of the subtropical ocean to both Rossby waves and Ekman pumping.

Equation (4) is commonly solved by either numerical calculation (Busalacchi and O'Brien 1980; Busalacchi et al. 1983) or integrating along characteristics (Gill and Clarke 1974; Meyers 1979; Kessler 1990). Here, however, we use a series of statistical techniques to isolate the wind stress curl effects [using singular value decomposition (SVD)] from large-scale propagating features [complex empirical orthogonal function (CEOF) analysis], and to further separate the propagating response into its forced and freely propagating components [multichannel singular spectrum analysis (M-SSA)]. Since our interest is on the interannual variability, and since the annual signal is weak over the eastern North Pacific (Goldenberg and O'Brien 1981; Kessler 1990), all analyses are applied to the deannualized model upper-layer thickness and wind stress curl fields.

a. Large-scale Ekman pumping

In this section, the interannual variability of the topmost model layer to wind stress curl forcing is examined. Equation (4) suggests that increases (decreases) in layer thickness should be associated with negative (positive) wind stress curl anomalies. Thus, any atmospheric response that acts to alter the gradients in the zonal or meridional wind stress will likewise force a response to the modeled upper layer thickness.

As discussed in Bretherton et al. (1992) and Wallace et al. (1992), an efficient way to isolate the dynamically linked response between two fields is to apply singular value decomposition analysis to the fields. Since we are interested in the associated temporal response of the two fields, SVD analysis is applied to the temporal cross-covariance matrix of the wind stress curl and the modeled upper-layer thickness. The upper-layer thickness (as opposed to the time rate of change of upper-layer thickness) is chosen to better represent the integrated effects of the wind stress curl. Results of the SVD analysis are presented in Fig. 2.

The first SVD mode (Fig. 2) represents a long term climatological signal with an associated jump in wind stress curl amplitude occurring between 1984 and 1986. However, the length of model results (16 yr) limits the ability to clearly determine the source of the signal and its implications. It is possible that the high variance associated with mode 1 (39%) is due to strongly coherent wind stress curl maxima in the vicinity of Hawaii or a change in the ECMWF/HR winds themselves (as noted by Hundermark et al. 1999). In either case, the overall large scale response is likely due to an interdecadal pattern not properly resolved by the time series used here.

The second SVD mode (Fig. 2), with 24% variance, depicts an interannual signal with a strong relationship between the wind stress curl and the modeled upper layer thickness (both spatially and temporally). For convenience, the upper-layer thickness temporal function has been multiplied by −1 to reveal the correspondence with the wind stress curl. As predicted by Eq. (4), a large positive (negative) wind stress curl anomaly is followed by an associated negative (positive) upper-layer thickness anomaly. Additionally, it should be of no surprise that the wind forcing contains more variability than the upper-layer thickness, owing itself to the slow response time of the ocean relative to the atmosphere.

The higher order SVD modes, modes 3 and 4 (not shown), represent additional sources of interannual variability, but with much lower variance (13% and 8%, respectively). These modes represent part of a propagating pattern associated with or resulting from SVD mode 2. The first four modes of the SVD analysis account for 82% of the overall squared covariance.

Having seen a covarying response between the upper-layer thickness and the wind stress curl, we consider the temporal nature of the response. Since the dynamically linked response has largest amplitude and is centered around 20°N, this latitude is chosen as a representative example throughout the remaining discussion. Hovmöller diagrams of the modeled

upper-layer thickness and the upper-layer thickness response associated with the wind stress curl for SVD mode 2 upstream of the Hawaiian Islands along 20°N (Fig. 3) reveal a distinct correspondence between the total and projected model upper-layer thickness.

The covarying SVD mode is clearly evident and compares well with the stationary component of the modeled upper-layer thickness. The interannual signal is pronounced in both with slight deviations in the total modeled upper-layer thickness. These deviations are associated with large-scale propagating features, such as long Rossby waves or extremely low frequency variability, as addressed in the following sections.

b. Propagating patterns

The second mechanism in Eq. (4) for modifying upper-layer thickness is advection of upper layer thickness gradients by large-scale propagating features, in this case Rossby waves. Complex empirical orthogonal function (CEOF) analysis (Shriver et al. 1991) isolates coherent propagating features with substantial amounts of variance. The CEOF analysis is calculated over the region 10°–50°N, 150°–78°W in an effort to retain coastally propagating features, unlike the SVD and M-SSA analyses.

The spatial and temporal representations of CEOF modes 1–3 show similar results to the SVD analysis. The dominant mode (not shown) reveals the same low frequency pattern as the SVD analysis, likely a longer term response to an interdecadal signature in the wind forcing. Again, though, the model time series does not allow for a direct analysis of this long timescale. Whatever the responsible mechanism may be, the probable result is a simple alteration of the background state upon which the interannual variability acts (Wang 1995; Wang and Ropelewski 1995).

The second most dominant CEOF mode (Fig. 4), encompassing 20% of the overall variance, represents the large scale Ekman pumping modes described using SVD in section 3a. The spatial function reveals a large amplitude response upstream of the Hawaiian Islands between 150° and 120°W and (for the most part) in phase but separated from the weak coastal response to its immediate east, suggesting separate dynamics are responsible for the coastal and interior ocean regions. This signal represents the dominant interannual signal over the region, with a period of roughly four years and corresponding to the El Niño events of 1982–83, 1986–87, and 1992–93. This signal represents large-scale wind forced Rossby waves.

This mode as well as higher modes (not shown) exhibit strong coastal propagation associated with ENSO related equatorially generated coastal Kelvin waves. Even though this signal propagates northward with the expected phase speed for a coastally trapped Kelvin wave (Fig. 4b), it is clearly independent of and much weaker than the interior wind-forced signal. Unlike mode 2, however, the interior free Rossby wave propagation seen in the higher modes is intricately connected with the coastal response, as expected. Additionally, an interference pattern along the coast causes a disruption and subsequent weakening of the coastal Kelvin wave response near 22°N. This response may be a manifestation of coastal geometry including the Gulf of California.

Prior to this study, the two key elements thought responsible for the interannual variability in the eastern subtropical North Pacific were Ekman pumping and low frequency, freely propagating Rossby waves. The results presented here suggest that the propagating features noted in Fig. 3 are not due to a coastally generated Rossby wave response, but rather to interior forcing west of 120°W as discussed in this and the previous section.

Thus, the CEOF analysis suggests large-scale propagating patterns emanating from both near (modes 3–5) and away from (mode 2) the boundary. East of 120°W, the signal emanates from the eastern boundary and propagates westward. This feature is a coastally generated long Rossby wave. The signal continues west of 120°W, but is less coherent (mode 3) and with potentially faster propagation speed. At 120°W, another signal becomes apparent (mode 2) and propagates rapidly (faster than the coastally generated wave) westward. This signal is associated with the interannual Ekman pumping described in SVD mode 2 and represents a wind-forced Rossby wave.

As is expected (Chelton and Davis 1982; Pares-Sierra and O'Brien 1989; Johnson and O'Brien 1990; Kessler 1990; Shriver et al. 1991; White 1994, Miller et al. 1997), the coastally propagating Kelvin waves produce Rossby waves along the North American coast that propagate westward into the basin. However, over the eastern subtropical North Pacific Ocean and away from the boundary, the coastally generated Rossby waves (modes 3–5) are of lower amplitude than the midbasin, wind-forced Rossby waves (mode 2). This feature has also been observed and discussed by Miller et al. (1997) who associate the large wind forcing anomalies with interannual fluctuations in the Aleutian low pressure system.

c. Forced atmosphere–ocean response

In this section, M-SSA is applied to the upper-layer thickness (ULT) and wind stress curl (WSC) fields in an attempt to gather more information about the propagating interannual features exhibited in the previous sections. M-SSA is a technique, analogous to both SVD and EOF analysis, aimed at determining oscillating modes of variability in a given dataset (Keppenne

and Ghil 1992; Vautard et al. 1992; Keppenne and Ghil 1993; Allen and Robertson 1996; Allen and Smith 1996). In essence, M-SSA filters the data along given channels (or frequency bands) and extracts the modes of variability with maximum variance. The result is a series of oscillating modes of variability that clearly distinguish between patterns of variability that might otherwise be indistinguishable.

M-SSA is applied to ULT and WSC fields independently, unlike SVD analysis, in which the cross-covariance matrix of the two fields is used. Thus, the results represent oscillating modes of variability for each individual field and cannot be assumed to be part of a coupled mode of variability a priori. Additionally, as before, the data here are preprocessed to remove the annual cycle in an effort to better extract the interannual signals of variability. A window of $m = 60$ months was chosen to highlight the interannual variability while reducing the impact of lower frequency (>60 month) variability. Finally, since it is representative of the region, only results along 20°N are shown.

M-SSA modes 1 and 2 (Fig. 5) are temporally and spatially lagged, indicating that they are part of a propagating mode. Similarly, modes 3 and 4 (Fig. 6) represent the second largest propagating mode and modes 5–10 (Fig. 7) represent the third largest propagating mode (at least for ULT). For the remainder of this discussion, we refer to these three modes as $RC_{1–2}$, $RC_{3–4}$, and $RC_{5–10}$, respectively (where RC represents the reconstructed mode).

The leading M-SSA mode ($RC_{1–2}$; Fig. 5) corresponds to the large-scale interannual signal seen in SVD and CEOF mode 2. The $RC_{1–2}$, containing 59% and 21% of the ULT and WSC variance respectively, represents oscillating modes in both WSC and ULT that propagate westward[1] at ~ 12 cm s^{-1} with WSC propagation leading ULT propagation by roughly 3 months. This is to be expected since the ULT anomalies represent the integrated effects of the anomalous wind stress curl. Additionally, both WSC and ULT modes exhibit strong quadrennial (~ 51 months) periods of oscillation.

The second leading mode, $RC_{3–4}$ (Fig. 6), represents the familiar low frequency signal seen in the SVD and CEOF analysis. Due to the nature of the M-SSA analysis, the signal is not well represented and must be ignored here.

The next substantial mode, $RC_{5–10}$ (Fig. 7), comprises numerous M-SSA modes.[2] M-SSA modes 5–10 collectively represent a quasi-biennial signal in both ULT and WSC. In the case of WSC, the signal carries 31% of the overall variance and represents primarily a standing mode of variability. Alternatively, the ULT response carries 16% of the overall variance and represents Rossby waves emanating from the eastern boundary and propagating westward freely with a phase speed of ~ 8 cm s^{-1}. Coupled with the CEOF analysis (section 3b; Fig. 4), this is further proof that these freely propagating Rossby waves and the wind-forced Rossby waves of $RC_{1–2}$ are distinct features of the interannual variability.

4. Discussion

Analysis of wind stress curl (WSC) and upper-layer thickness (ULT) anomalies have revealed several significant results. First, on interannual timescales, the leading order variability in the eastern subtropical North Pacific Ocean is attributed to large-scale variability in the wind stress curl and its associated Ekman pumping. The Ekman pumping anomalies give rise to wind-forced Rossby waves. Second, the WSC-related Ekman pumping and wind-forced Rossby waves both propagate westward at phase speeds of roughly 12 cm s^{-1}, with WSC leading Rossby wave propagation by about 3 months. Third, higher order interannual variability can be attributed to freely propagating Rossby waves generated at the eastern boundary. These freely propagating waves, with phase speeds (~ 8 cm s^{-1}) consistent with linear theory, are a distinct oceanic feature and, other than their generation, are not associated with the local Ekman pumping.

In addition to interannual WSC and ULT variability, an interdecadal mode (IDM) of variability is shown to exist over the same region. SVD and CEOF analysis reveal the IDM to be a leading order source of variability, but lack of sufficient temporal data limits the extent to which this feature can be adequately examined in the present study. However, the feature is consistent with interdecadal variability and amplifications in the Aleutian low and should be studied further.

It is worth noting that neither the model nor the techniques used are predisposed to the interannual variability seen in the eastern subtropical North Pacific. The fact that the modeled ULT variability matches well with the simple quasigeostrophic theory utilized here and by previous authors provides added evidence to the already hypothesized nature of the interannual variability, while simultaneously providing further proof of the ability of numerical models, and the NLOM in particular, to reproduce the observed oceanic interannual variability.

The results presented in this study are consistent with those of Miller et al. (1997), White et al. (1998), and White (2000). Namely, SVD, CEOF, and M-SSA results suggest that interannual variations in the interior eastern subtropical North Pacific Ocean are linked with large-scale fluctuations in the wind stress curl. At the same time, unlike the previous authors, the

results presented here reveal two distinct forms of westward propagating Rossby waves, the first of which is a weak boundary generated wave with phase speed consistent with that of linear theory and the other which is wind forced and faster, consistent with the theory of White (1977) and Qiu et al. (1997). Unfortunately, since the model used here is purely hydrodynamic, questions regarding the positive feedback mechanism of White et al. (1998) and White (2000) are beyond the scope of the current study and are left to future research.

It is also shown that although these two distinct Rossby wave forms coexist, the nature and magnitude of the wind forced Rossby waves masks the effects of the freely propagating Rossby waves, at least on interannual time scales and in the eastern subtropical North Pacific, as observed by Miller et al. (1997). Although the model includes nonlinear features and processes (e.g., advection and mesoscale eddies), the leading order response on both interdecadal and interannual timescales is primarily linear. These results support the notion that extratropical wind stress curl variability plays an important role in midlatitude interannual ocean variability.

The events described have potentially large impacts at all timescales for not only oceanic large and mesoscale variability, but also on biological/ecological productivity over a vast area of the eastern Pacific Ocean. As such, further effort should be placed on examining the features, discerning the nature of its variability, and studying its effects on marine ecosystems.

Acknowledgments

This research was conducted under National Aeronautics and Space Administration (NASA) Grant NGT5-30158. All research was completed while A. P. Leonardi was a NASA Earth System Science Graduate Research Fellow at The Florida State University (FSU). The numerical simulations were performed on the Cray Y-MP M98/82048 at the Los Alamos National Laboratory, Los Alamos, New Mexico, under Naval Research Laboratory Grant N00014-94-1-G918 and grants of computer time from the Department of Defense (DoD) High Performance Computing Modernization Program (HPCMP). Our deepest gratitude goes to Mr. E. Joseph Metzger, of NRL Stennis Space Center, for numerous discussions regarding the NLOM and the entire NRL oceanography division for their continued support and use of the NLOM. Special thanks is extended to Dr. William Dewar of FSU and Dr. Antonio Busalacchi of the Earth System Science Interdisciplinary Center at the University of Maryland, whose insightful comments, questions, and support greatly enhanced this research. COAPS receives its base support from the Physical Oceanography Section of the Office of Naval Research through a Secretary of the Navy Grant to J. J. O'Brien.

REFERENCES

Allen M. R., and A. W. Robertson, 1996: Distinguishing modulated oscillations from coloured noise in multivariate datasets. *Climate Dyn.*, **12**, 775–784. Find this article online

Allen M. R., and L. A. Smith, 1996: Monte Carlo SSA: Detecting irregular oscillations in the presence of coloured noise. *J. Climate*, **9**, 3373–3404. Find this article online

Bretherton C. S., C. Smith, and J. M. Wallace, 1992: An intercomparison of methods for finding coupled patterns in climate data. *J. Climate*, **5**, 541–560. Find this article online

Busalacchi A. J., and J. J. O'Brien, 1980: The seasonal variability in a model of the tropical Pacific. *J. Phys. Oceanogr.*, **10**, 1929–1951. Find this article online

Busalacchi A. J., K. Takeuchi, and J. J. O'Brien, 1983: Interannual variability of the equatorial Pacific, revisited. *J. Geophys. Res.*, **88**, 7551–7562. Find this article online

Chelton D. B., and R. E. Davis, 1982: Monthly mean sea-level variability along the west coast of North America. *J. Phys. Oceanogr.*, **12**, 757–784. Find this article online

Chelton D. B., and M. G. Schlax, 1996: Global observations of oceanic Rossby waves. *Science*, **272**, 234–238. Find this article online

Dewar W. K., 1998: On “too fast” planetary waves in the general circulation. *J. Phys. Oceanogr.*, **28**, 1739–1758. Find this article online

ECMWF,, 1995: User guide to ECMWF products. ECMWF Meteor. Bull. M3.2, 39 pp.

Gill A. E., 1982: *Atmosphere–Ocean Dynamics*. Academic Press, 662 pp.

Gill A. E., and A. J. Clarke, 1974: Wind induced upwelling, coastal currents and sea-level changes. *Deep-Sea Res.*, **21**, 321–345. Find this article online

Goldenberg S. B., and J. J. O'Brien, 1981: Time and space variability of the tropical Pacific wind stress. *Mon. Wea. Rev.*, **109**, 1190–1207. Find this article online

Hackert E. C., A. J. Busalacchi, and R. Murtugudde, 2001: A wind comparison study using an ocean general circulation model for the 1997–1998 El Niño. *J. Geophys. Res.*, **106**, 2345–2362. Find this article online

Hellerman S., and M. Rosenstein, 1983: Normal monthly wind stress over the world ocean with error estimates. *J. Phys. Oceanogr.*, **13**, 1093–1104. Find this article online

Hundermark B. A., H. E. Hurlburt, E. J. Metzger, and J. F. Shriver, 1999: A comparison of wind stresses derived from archived operational European Centre for Medium-Range Weather Forecasts 1000 mb winds and Florida State University psuedo stresses over the tropical Pacific Ocean, 1981–1993. Naval Res. Lab. Rep. NRL/FR/7320-99-9643, Washington, DC, 40 pp.

Hurlburt H. E., and J. D. Thompson, 1980: A numerical study of the Loop Current intrusions and eddy shedding. *J. Phys. Oceanogr.*, **10**, 1611–1651. Find this article online

Hurlburt H. E., A. J. Wallcraft, W. J. Schmitz Jr., P. J. Hogan, and E. J. Metzger, 1996: Dynamics of the Kuroshio/Oyashio current system using eddy-resolving models of the North Pacific Ocean. *J. Geophys. Res.*, **101**, 941–976. Find this article online

Jacobs G. A., H. E. Hurlburt, J. C. Kindle, E. J. Metzger, J. L. Mitchell, W. J. Teague, and A. J. Wallcraft, 1994: Decade-scale trans-Pacific propagation and warming effects of an El Niño anomaly. *Nature*, **370**, 360–363. Find this article online

Johnson M. A., and J. J. O'Brien, 1990: The northeast Pacific Ocean response to the 1982–1983 El Niño. *J. Geophys. Res.*, **95**, 7155–7166. Find this article online

Kang Y. Q., and L. Magaard, 1980: Annual baroclinic Rossby waves in the central North Pacific. *J. Phys. Oceanogr.*, **10**, 1159–1167. Find this article online

Keppenne C. L., and M. Ghil, 1992: Adaptive spectral analysis and prediction of the Southern Oscillation index. *J. Geophys. Res.*, **97**, 20449–20454. Find this article online

Keppenne C. L., 1993: Adaptive filtering and prediction of noisy multivariate signals: An application to subannual variability in atmospheric angular momentum. *Int. J. Bifurcation Chaos*, **3**, 625–634. Find this article online

Kessler W. S., 1990: Observations of long Rossby waves in the northern tropical Pacific. *J. Geophys. Res.*, **95**, 5183–5217. Find this article online

Killworth P. D., D. B. Chelton, and R. A. deZoeke, 1997: The speed of observed and theoretical extra tropical planetary waves. *J. Phys. Oceanogr.*, **27**, 1946–1966. Find this article online

Magaard L., 1983: On the potential energy of baroclinic Rossby waves in the North Pacific. *J. Phys. Oceanogr.*, **13**, 38–42. Find this article online

Mesinger F., and A. Arakawa, 1976: Numerical methods used in atmospheric models. GARP Publications Series 14, WMO/ICSU Joint Organizing Committee, 64 pp.

Metzger E. J., and H. E. Hurlburt, 1996: Coupled dynamics of the South China Sea, the Sulu Sea and the Pacific Ocean. *J. Geophys. Res.*, **101**, 12331–12352. Find this article online

Meyers G., 1975: Seasonal variation in transport of the Pacific North Equatorial Current relative to the wind field. *J. Phys. Oceanogr.*, **5**, 442–449. Find this article online

Meyers G., 1979: On the annual Rossby wave in the tropical North Pacific Ocean. *J. Phys. Oceanogr.*, **9**, 663–674. Find this article online

Miller A. J., W. B. White, and D. R. Cayan, 1997: North Pacific thermocline variations on ENSO timescales. *J. Phys. Oceanogr.*, **27**, 2023–2039. Find this article online

Mitchell J. L., W. J. Teague, G. A. Jacobs, and H. E. Hurlburt, 1996: Kuroshio Extension dynamics from satellite altimetry and a model simulation. *J. Geophys. Res.*, **101**, 1045–1058. Find this article online

Murray C. P., S. L. Morey, and J. J. O'Brien, 2001: Interannual variability of upper ocean vorticity balances in the Gulf of Alaska. *J. Geophys. Res.*, **106**, 4479–4491. Find this article online

NOAA,, 1986: ETOP05 digital relief of the surface of the earth. Natl. Geophys. Data Center Data Announcement 86-MGG-07, 1 p.

Pares-Sierra A., and J. J. O'Brien, 1989: The seasonal and interannual variability of the California Current system. *J. Geophys. Res.*, **94**, 3159–3180. Find this article online

Qiu B., W. Mao, and P. Müller, 1997: Propagation and decay of forced and free baroclinic Rossby waves in off-equatorial oceans. *J. Phys. Oceanogr.*, **27**, 2405–2417. Find this article online

Shriver J. F., and H. E. Hurlburt, 1997: The contribution of the global thermohaline circulation to the Pacific to Indian Ocean throughflow via Indonesia. *J. Geophys. Res.*, **102**, 5491–5511. Find this article online

Shriver J. F., M. A. Johnson, and J. J. O'Brien, 1991: Analysis of remotely forced oceanic Rossby waves off California. *J. Geophys. Res.*, **96**, 749–757. Find this article online

Stommel H., 1957: A survey of ocean current theory. *Deep-Sea Res.*, **4**, 149–184. Find this article online

Subrahmanyam B., 1998: A study of the Indian Ocean circulation using satellite observations and model simulations. Ph.D. thesis, University of Southhampton, 213 pp.

Tourre Y. M., Y. Kushnir, and W. B. White, 1999: Evolution and variability in sea level pressure, sea surface temperature, and upper ocean temperature over the Pacific Ocean. *J. Phys. Oceanogr.*, **29**, 1528–1541. Find this article online

Vautard R., P. Yiou, and M. Ghil, 1992: Singular spectrum analysis: A toolkit for noisy and chaotic series. *Physica D*, **58**, 95–126. Find this article online

Wallace J. M., C. Smith, and C. S. Bretherton, 1992: Singular value decomposition of wintertime sea surface temperature and 500-mb height anomalies. *J. Climate*, **5**, 561–576. Find this article online

Wallcraft A. J., 1991: The Navy layered ocean model user's guide. NOARL Rep. 35, Naval Research Laboratory, Stennis Space Center, MS, 21 pp.

Wang B., 1995: Interdecadal changes in El Niño onset in the last four decades. *J. Climate*, **8**, 267–285. Find this article online

Wang X. L., and C. F. Ropelewski, 1995: An assessment of ENSO-scale secular variability. *J. Climate*, **8**, 1584–1599. Find this article online

White W. B., 1977: Annual forcing of baroclinic long waves in the tropical North Pacific. *J. Phys. Oceanogr.*, **7**, 50–61. Find this article online

White W. B., 1978: A wind-driven model experiment of the seasonal cycle of the main thermocline in the interior midlatitude North Pacific. *J. Phys. Oceanogr.*, **8**, 818–824. Find this article online

White W. B., 1994: Slow El Niño–Southern Oscillation boundary waves. *J. Geophys. Res.*, **99**, 22737–22751. Find this article online

White W. B., 2000: Tropical coupled Rossby waves in the Pacific ocean–atmosphere system. *J. Phys. Oceanogr.*, **30**, 1245–1264. Find this article online

White W. B., and J. P. McCreary, 1974: Eastern intensification of ocean spin-down: Application to El Niño. *J. Phys. Oceanogr.*, **4**, 295–303. Find this article online

White W. B., and D. R. Cayan, 2000: A global El Niño–Southern Oscillation wave in surface temperature and pressure and its interdecadal modulation from 1900 to 1997. *J. Geophys. Res.*, **105**, 11223–11242. Find this article online

White W. B., G. A. Meyers, J. R. Donguy, and S. E. Pazan, 1985: Short-term climatic variability in the thermal structure of the Pacific Ocean during 1979–1982. *J. Phys. Oceanogr.*, **15**, 917–935. Find this article online

White W. B., Y. Chao, and C. K. Tai, 1998: Coupling of biennial oceanic Rossby waves with the overlying atmosphere in the Pacific basin. *J. Phys. Oceanogr.*, **28**, 1236–1251. Find this article online

Zamudio L., A. P. Leonardi, S. D. Meyers, and J. J. O'Brien, 2001: ENSO and eddies on the southwest coast of Mexico. *Geophys. Res. Lett.*, **28**, 13–16. Find this article online

---

Figures

Click on thumbnail for full-sized image.

FIG. 1. First (a, b, and c) and second (d, e, and f) mode EOF spatial amplitude functions of the unfiltered NLOM (a, d) and TOPEX/Poseidon (T/P) (c, f) sea surface height along with their associated principal components [b, e; NLOM: black line, T/P: red line]. Mode 1 (2) represents 16% (12%) and 22% (12%) of the overall variance for the NLOM and T/P SSH, respectively

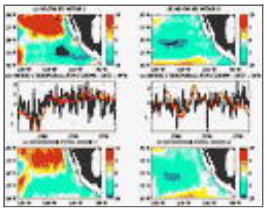

Click on thumbnail for full-sized image.

FIG. 2. First (a, b, and c) and second (d, e, and f) mode SVD eigenvectors of the monthly mean NLOM upper-layer thickness (a, d) and ECMWF/HR monthly wind stress curl (c, f) along with their associated eigenfunctions [b, e; NLOM: red line, ECMWF/HR: black line] accounting for 39% and 24% of the overall squared covariance, respectively

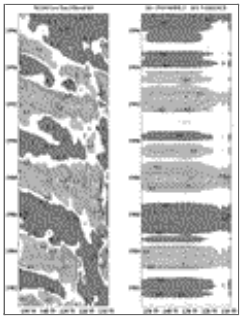

Click on thumbnail for full-sized image.

FIG. 3. Modeled upper-layer thickness anomaly (left) and upper-layer thickness anomaly associated with the SVD mode 2 (right) along 20°N upstream of the Hawaiian Islands. For comparison purposes, the modeled upper-layer thickness is normalized in a manner consistent with the SVD analysis. The covarying standing mode (right) represents 24% of the overall squared covariance

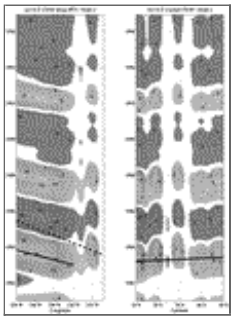

Click on thumbnail for full-sized image.

FIG. 4. Reconstructed upper-layer thickness for CEOF analysis mode 2, representing 20% of the overall variance for the region, along (a) 20°N revealing wind forced Rossby waves in the interior away from the coast, and along (b) the North American coast from 10° to 50°N showing coastally propagating Kelvin waves. Superimposed on (a) are the phase lines for freely propagating (dashed) and wind forced (solid) Rossby waves, and on (b) the expected phase speed for coastally trapped Kelvin waves (solid). Units for the ULT anomalies are meters

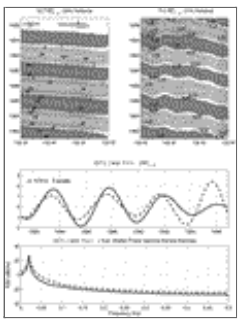

Click on thumbnail for full-sized image.

FIG. 5. M-SSA results for upper-layer thickness (ULT) and wind stress curl (WSC). Interannual variability is represented by reconstructed components 1 and 2 ($RC_{1–2}$) for both ULT, carrying 59% of the variance (top left), and WSC, carrying 21% of the variance (top right), respectively. The reconstructed principal components (middle panel) are highly correlated, $r = -0.76$ at the 99% confidence level, with WSC variations leading ULT by 3 months. Both ULT (bottom panel, solid line) and WSC (bottom panel, dashed line) show strong spectral peaks in the interannual band with frequencies corresponding to ~ 51 months

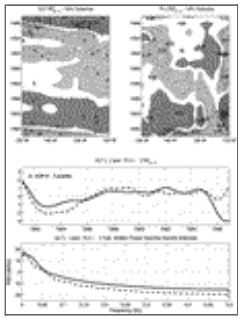

Click on thumbnail for full-sized image.

FIG. 6. As in Fig. 5 but for M-SSA reconstructed modes 3 and 4 ($RC_{3–4}$). A clear interdecadal signal is exhibited with slight propagation. Both signals are highly correlated in time ($r = -0.59$ at the 99% level) with frequency peaks in the interdecadal bands

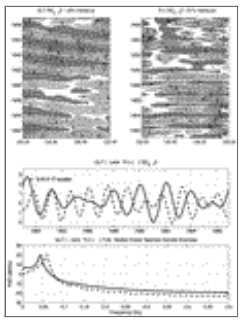

Click on thumbnail for full-sized image.

FIG. 7. As in Fig. 5, but for M-SSA reconstructed modes 5–10 ($RC_{5–10}$). Quasi-biennial variability is exhibited for both ULT and WSC anomalies, but with low correlation. The two modes represent differing signals with ULT anomalies being biennial Rossby waves with a period of 24 months, and WSC anomalies representing a quasi-biennial standing mode with period of 17 months

Corresponding author address: Dr. Alan P. Leonardi, Earth System Science Interdisciplinary Center, University of Maryland, 2231 Computer and Space Sciences Building, College Park, MD 20742-2465. E-mail: leonardi@essic.umd.edu

[1] In the above analysis, phase speeds are estimated by constructing a longitude lag/time lag correlation matrix similar to that presented by White et al. (1985). In this method, a correlation matrix is created for the given longitude–time (Hovmöller) plot and a best line fit is calculated to determine the propagation speed.

[2] Since the individual M-SSA modes 5–10 all represent similar temporal and spatial characteristics with closely corresponding eigenvalues, they are chosen to represent a single mode of variability.

top